ON EXTRAPOLATION IN MATERIAL PROPERTY REGRESSION

Anonymous authors
Paper under double-blind review

ABSTRACT

Deep learning methods have yielded exceptional performances in material property regression (MPR). However, most existing methods operate under the assumption that the training and test are independent and identically distributed (i.i.d.). This overlooks the importance of extrapolation - predicting material properties beyond the range of training data - which is essential for advanced material discovery, as researchers strive to identify materials with exceptional properties that exceed current capabilities. In this paper, we address this gap by introducing a comprehensive benchmark comprising seven tasks specifically designed to evaluate extrapolation in MPR. We critically evaluate existing methods including deep imbalanced regression (DIR) and regression data augmentation (DA) methods, and reveal their limitations in extrapolation tasks. To address these issues, we propose the Matching-based EXtrapolation (MEX) framework, which reframes MPR as a material-property matching problem to alleviate the inherent complexity of the direct material-to-label mapping paradigm for better extrapolation. Our experimental results show that MEX outperforms all existing methods on our benchmark and demonstrates exceptional capability in identifying promising materials, underscoring its potential for advancing material discovery.

1 INTRODUCTION

Material property regression (MPR), the task of predicting continuous material property values, plays a critical role in material discovery across diverse applications such as catalysts and batteries. Traditional density functional theory (DFT)-based methods, while accurate, are often computationally prohibitive for large-scale screening. To address this challenge, deep learning models (Xie & Grossman, 2018; Schütt et al., 2021; Yan et al., 2022; Liao et al., 2024; Shoghi et al., 2024) have emerged as efficient alternatives, providing rapid predictions that facilitate the identification of promising material candidates for further validation through detailed simulations or experiments.

Predicting material properties beyond the range covered by training data, known as extrapolation, is a crucial yet under-explored area in deep learning-based MPR. Materials scientists strive to discover materials with superior properties compared to existing ones, such as organic light-emitting diodes (OLEDs) with extreme color purity (Xu et al., 2020; Kim & Yasuda, 2022), semiconductor materials with extraordinary thermodynamic stability (Castelli et al., 2012a;b) (Figure 1), and more. In this context, the extrapolation ability of deep learning models becomes crucial, as these novel properties often do not exist in currently known materials. However, most existing MPR benchmarks (Dunn et al., 2020; Choudhary et al., 2024; Chang et al., 2022) assume that both training and testing set are independent samples from an identical distribution (i.e. *i.i.d.* samples), limiting exploration of extrapolation challenges.

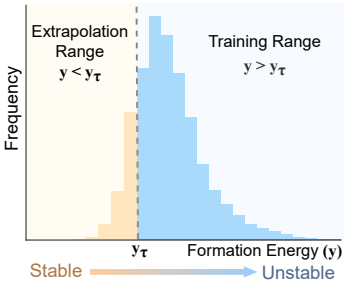

Figure 1: Extrapolation in MPR (for Formation Energy), which aims to generalize to label values ($y < y_\tau$) outside the training label range ($y > y_\tau$).

To address this gap, in this paper, we curate a comprehensive extrapolation benchmark consisting of seven datasets sourced from `Matminer` (Ward et al., 2018), accompanied by well-defined train/validation/test splits based on real-

world material applications. We then carefully evaluate the existing methods under a wide range of (1) backbones, including representative equivariant geometric GNNs such as PaiNN (Schütt et al., 2021) and EquiformerV2 (Liao et al., 2024); (2) training algorithms, including classic ERM, deep imbalanced regression (DIR) methods (Yang et al., 2021; Gong et al., 2022; Ren et al., 2022; Keramati et al., 2024), and data augmentation techniques (Yao et al., 2022; Kaufman & Azencot, 2024); and (3) metrics, such as mean absolute error (MAE) and error geometric mean (GM). Given that structure-to-property mappings are governed by intricate quantum mechanical interactions, and neural networks often struggle to capture complex non-linearity beyond the scope of training data (Xu et al., 2021), it is unsurprising that these methods struggle with extrapolation tasks in MPR, highlighting the need for more tailored methodologies for this challenge.

In response, we propose **M**atching-based **EX**trapolation (MEX), a novel framework that reframes MPR as a material-property matching problem, aimed at simplifying the complexity of target functions to enhance model extrapolation. Our intuition is that matching - focusing on the proximity between material and property representations rather than precise value predictions - reduces learning difficulty and improves extrapolation. Specifically, MEX employs two complementary training objectives to learn aligned feature spaces for material and property representation matching. First, it performs absolute matching optimization using negative cosine similarity loss, which pulls paired material and label representations closer together. Second, MEX leverages Noise Contrastive Estimation (NCE) (Gutmann & Hyvärinen, 2010) to force the model to distinguish between target and noisy labels, thus capturing fine-grained relative matching relationships. Within the well-aligned latent spaces, MEX predicts by optimizing for the nearest target value for a given sample. Experiments show that MEX not only achieves the best performance on our benchmark but also exhibits extraordinary detection capability for promising materials, demonstrating superior extrapolation capabilities and potential for more robust material discovery.

Our contributions are summarized as follows:

- We highlight the critical importance of extrapolation in MPR, an area that has been previously understudied yet holds significant implications for realistic material design scenarios.
- We curate a comprehensive benchmark specifically designed to evaluate extrapolation in material properties regression, and thoroughly investigate the effectiveness of deep imbalanced regression (DIR) and regression data augmentation (DA) methods on extrapolation tasks, revealing their limitations in handling the complexities of MPR.
- We propose MEX, a simple yet effective framework that substantially enhances extrapolation capabilities, achieving state-of-the-art performance on our benchmark.

2 RELATED WORK

Material property prediction. Recent years have witnessed the tremendous impact of deep learning on predicting material properties (Schütt et al., 2018; Yan et al., 2022; Shoghi et al., 2024). Considering the 3D atomic systems' essence of material data, numerous studies have aimed to enhance neural architectures to effectively capture the intrinsic physical symmetries of such data. SchNet (Schütt et al., 2018) and CGCNN (Xie & Grossman, 2018) pioneered the use of graph neural networks for 3D atomic systems, which modeled the pairwise atomic distance variant with regard to Euclidean transformations. Since then, a body of research has focused on encoding higher-order geometric invariants (Klicpera et al., 2020; Gasteiger et al., 2021; Yan et al., 2022) and equivariants (Schütt et al., 2021; Passaro & Zitnick, 2023; Liao et al., 2024).

Another area of focus lies in pre-training to learn transferable material representations (Zhang et al., 2023; Shoghi et al., 2024; Song et al., 2024). For instance, Shoghi et al. (2024) propose joint pre-training on force and energy prediction tasks across different chemical domains and show impressive transfer performance to downstream tasks. Song et al. (2024) employed a self-supervised pre-training task via crystal structure reconstruction based on diffusion models. Orthogonal to existing research efforts, our work focuses on the overlooked issue of extrapolation in MRP and approaches it from a unique training strategy perspective, which can use any model architecture and pre-trained model as backbones.

Imbalanced regression. Imbalanced regression aims to learn continuous targets from imbalanced data where certain target values are scarce, and generalize to the entire target range. Early

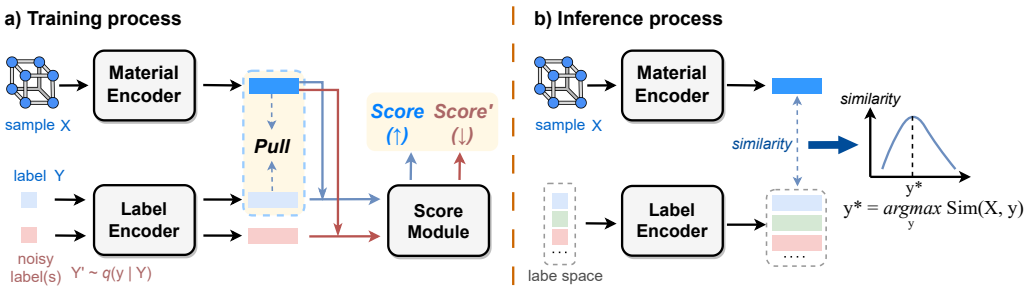

Figure 2: The framework of MEX. (a) MEX begins by drawing noisy labels from a noise distribution. Both samples and labels are embedded into the feature space, where MEX pulls the sample and its target label closer together. Noise Contrastive Estimation loss is then applied to refine this feature space by maximizing the score between the sample and its correct label while minimizing the scores between the sample and noisy labels. (b) MEX predicts the label by identifying the most similar one to the sample in the learned feature space.

works (Torgo et al., 2013; Branco et al., 2017) use over-sampling techniques by synthesizing samples for minority targets. DenseWeight (Steininger et al., 2021) and LDS (Yang et al., 2021) adopted a similar approach of using kernel density estimation to estimate the 'real' label density distribution, and subsequently re-weighting the samples accordingly. VIR (Wang & Wang, 2023) produces *balanced probabilistic representations* by mixing data with similar targets and modulates the distribution to impose probabilistic reweighting on imbalanced data. BalancedMSE (Ren et al., 2022) identifies the label imbalance that MSE carries into prediction and mitigates it by restoring a balanced prediction distribution. Current state-of-the-art approaches encourage preserving label-space relationships in the feature space, such as label similarity orders (Gong et al., 2022), relative similarities (Keramati et al., 2024) and topology (Zhang et al., 2024). Unlike imbalanced regression, extrapolation pursues generalization to the label range beyond the training support. Therefore, existing DIR methods are suboptimal for extrapolation. In contrast, we focus specifically on extrapolation and propose a novel training scheme that performs prediction by matching material and target in a unified latent space, rather than conventional single-point estimation used by those DIR methods.

3 METHODOLOGY

3.1 PROBLEM DEFINITION

We define MPR extrapolation tasks as predicting unobserved material property values that lie outside the training label range. Formally, let the input space and label space be denoted as $\mathcal{X}$ and $\mathcal{Y}$, where $\mathcal{X}$ contains the structural data of materials, and $\mathcal{Y} \subset \mathbb{R}$ corresponds to a continuous range of labels. The training domain and target domain are respectively defined as $\mathcal{D}_{\text{train}} = \{(x, y) \mid (x, y) \in \mathcal{X} \times \mathcal{Y}_{\text{train}}\}$ and $\mathcal{D}_{\text{target}} = \{(x, y) \mid (x, y) \in \mathcal{X} \times \mathcal{Y}_{\text{target}}\}$, where $\mathcal{Y}_{\text{train}}$ and $\mathcal{Y}_{\text{target}}$ are two disjoint subspaces of $\mathcal{Y}$, i.e.,

$$\mathcal{Y}_{\text{target}} \subset \left\{y \in \mathcal{Y} \mid y > \max(\mathcal{Y}_{\text{train}}) \vee y < \min(\mathcal{Y}_{\text{train}})\right\}$$

The goal of extrapolation is to learn a model $f : \mathcal{X} \to \mathcal{Y}$ that minimizes the extrapolation error $\mathbb{E}_{(x,y)\sim\mathcal{D}_{\text{target}}}[\ell(f(x), y)]$, where $\ell : \mathbb{R} \times \mathbb{R} \to \mathbb{R}$ is the loss function. Note that the model can only utilize $\mathcal{D}_{\text{train}}$ without further adapting to $\mathcal{D}_{\text{target}}$ during training.

3.2 MATCHING-BASED EXTRAPOLATION

In contrast to directly mapping materials to properties, we argue that learning the matching relationship between them presents a simpler learning target, facilitating model generalization in previously unseen label ranges. Given a training set comprising N examples $D_{\text{train}} = \{(x_i, y_i)\}_{i=1}^{N}$, we aim to learn a binary matching function $\mathcal{M}(x, y)$ that output high values for a paired sample x and label y, while assigning lower values to unpaired ones. MEX parameterizes $\mathcal{M}(x, y)$ as $\text{Sim}(\mathcal{E}_s(x), \mathcal{E}_l(y))$, where $\mathcal{E}_s(\cdot) : \mathcal{X} \to \mathbb{R}^d$ represents the material encoder, $\mathcal{E}_l(\cdot) : \mathbb{R} \to \mathbb{R}^d$ represents the label encoder, and $\text{Sim}(\cdot, \cdot) : \mathbb{R}^d \times \mathbb{R}^d \to \mathbb{R}$ is the cosine similarity between two vectors. We denote the

encoded material and label as $\boldsymbol{z}^s$ and $\boldsymbol{z}^l$, respectively. Variables with subscript i correspond to the i-th example in the training set.

The overall architecture of MEX is illustrated in Figure 2. In the following, we first outline the training process in Section 3.2.1, which aligns the sample and label feature spaces to capture their matching relationship from both absolute and relative perspectives. We then describe how to reformulate the regression to a matching problem in Section 3.2.2, which optimizes for the most matching label for a given sample based on the learned matching function.

3.2.1 TRAINING STAGE

In this section, we will introduce two training objectives for learning the sample-label matching relationship.

Absolute matching optimization. Since samples and labels are encoded separately, we optimize the cosine similarity between each $\boldsymbol{z}_i^s$ and $\boldsymbol{z}_i^l$ to align their feature spaces (left side, Figure 2-a), capturing the absolute material-property matching relationship:

$$\mathcal{L}_{abs,i} = -\frac{\boldsymbol{z}_i^s \cdot \boldsymbol{z}_i^l}{||\boldsymbol{z}_i^s|| \times ||\boldsymbol{z}_i^l||}, \tag{1}$$

and the total loss of N samples is

$$\mathcal{L}_{abs} = \frac{1}{N}\sum_{i=1}^{N}\mathcal{L}_{abs,i}. \tag{2}$$

Relative matching optimization. Although $\mathcal{L}_{abs}$ enables the model to capture the matching relationship between a sample and its corresponding target value, it ignores relationships with other values, which is crucial for continuous label regression. To achieve this, we adopt the Noise Contrastive Estimation (NCE) (Gutmann & Hyvärinen, 2010) loss:

$$\mathcal{L}_{nce,i} = -\log \frac{\exp\left\{\mathcal{S}\left(\boldsymbol{z}_i^s, \boldsymbol{z}_{(i,0)}^l\right) - \log q\left(y_{(i,0)} \mid y_i\right)\right\}}{\sum_{m=0}^{M}\exp\left\{\mathcal{S}\left(\boldsymbol{z}_i^s, \boldsymbol{z}_{(i,m)}^l\right) - \log q\left(y_{(i,m)} \mid y_i\right)\right\}}, \tag{3}$$

where $\mathcal{S}(\cdot,\cdot) : \mathbb{R}^d \times \mathbb{R}^d \to \mathbb{R}$ refers to a non-linear score module (right side, Figure 2-a), which outputs the score of a sample representation and a label representation. We define $y_{(i,0)} \coloneqq y_i$ and $\{y_{(i,m)}\}_{m=1}^{M}$ as M noisy label values sampled from the noise distribution $q(y|y_i)$. Their corresponding label representations are denoted as $\{\boldsymbol{z}_{(i,m)}^l\}_{m=0}^{M}$. The noise distribution is modeled as a mixture of K Gaussions centered at y_i following Gustafsson et al. (2020):

$$q(y|y_i) = \frac{1}{K}\sum_{k=1}^{K}\mathcal{N}(y; y_i, \sigma_k^2). \tag{4}$$

The final NCE loss of the training samples is

$$\mathcal{L}_{nce} = \frac{1}{N}\sum_{i=1}^{N}\mathcal{L}_{nce,i}. \tag{5}$$

Minimizing $\mathcal{L}_{nce}$ encourages the model to distinguish the target value from noisy values, thereby capturing the fine-grained relative relationships between samples and labels more effectively.

By combining the absolute and relative matching optimization, the total training objective is:

$$\mathcal{L} = \mathcal{L}_{nce} + \lambda\mathcal{L}_{abs}, \tag{6}$$

where λ is a trade-off parameter.

3.2.2 INFERENCE STAGE

During inference, the problem of predicting the target value of a sample x can be formulated as finding a label $y^\star$ that best matches x. Based on the learned matching function, the prediction $y^\star$ can thus be obtained by directly maximizing the matching function $\mathcal{M}(x, y)$ w.r.t. y.

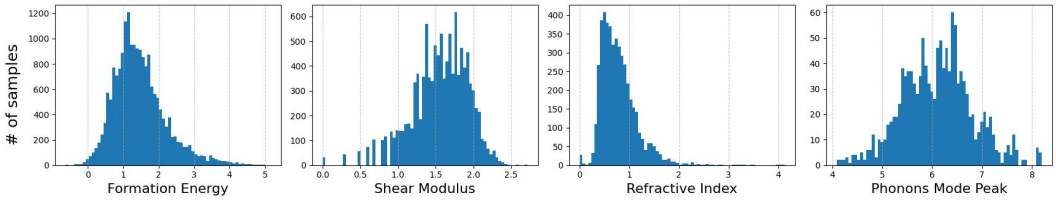

Figure 3: Overview of the label distribution for the origin MPR datasets. The X-axis denotes the respective property values. They were divided into seven benchmark datasets.

Table 1: Details of the seven benchmark datasets.

Property	Num samples	Original source	Split configuration	Training label range	Val label range	Test label range
Formation Energy	18982	Castelli et al. (2012a)	bottom	[1.06, 5.16]	[0.76, 1.06]	[-0.64, 0.76]
Shear Modulus	10987	Jain et al. (2013)	bottom	[1.4, 2.72]	[1.18, 1.4]	[0, 1.18]
			top	[0, 1.78]	[1.78, 1.93]	[1.93, 2.72]
Refractive Index	4764	Petousis et al. (2017)	bottom	[0.56, 4.13]	[0.45, 0.56]	[0, 0.45]
			top	[0, 0.9]	[0.9, 1.11]	[1.11, 4.13]
Phonons Mode Peak	1265	Petretto et al. (2018)	bottom	[5.72, 8.2]	[5.41, 5.72]	[4.09, 5.41]
			top	[4.09, 6.45]	[6.45, 6.79]	[6.8, 8.2]

We estimate $y^\star = \text{argmax}_y \mathcal{M}(x, y)$ with the Monte Carlo sampling-based stochastic optimization method (Homem-de Mello & Bayraksan, 2014), which iteratively refine a candidate label set $Y_{\text{cand}} = \{y_c\}_{c=1}^{C}$ based on probabilistic evaluations. This approach balances exploration and exploitation, allowing the matching values of candidate labels to converge toward high values. Finally, the prediction of x is $y^\star = \text{argmax}_{y \in Y_{\text{cand}}} \mathcal{M}(x, y)$. The detailed algorithm for the inference procedure is provided in Appendix A.2.

4 BENCHMARKING EXTRAPOLATION IN MPR

4.1 DATASET

We curated a range of extrapolative MPR benchmark datasets using four datasets from `Matminer` (Ward et al., 2018) covering the following properties: formation energy, shear modulus, refractive index, and phonons mode peak, with dataset size ranging from 1,265 to 18,928. Figure 3 shows the label distribution of the raw datasets and more dataset characteristics are provided in Table 5. These datasets are split into train/validation/test sets with a ratio of 7:1.5:1.5. Rather than employing conventional partition methods like random splitting, we selected extreme target values for extrapolation evaluation. Specifically, each dataset is first sorted by the property values, and the top (or bottom) 15%, along with the second top (or bottom) 15%, were used as the test and validation sets, respectively. Whether we select the top or bottom extremes is determined by the specific property desired in material design scenarios. For example, lower formation energy indicates higher material stability, prompting researchers to search for materials with extremely low formation energies. Thus, for such properties, we select the bottom values for evaluation. For properties where both low and high values are of interest, e.g., shear modulus, the dataset is split with the top and bottom configuration once each to ensure comprehensive evaluation across the spectrum. Details of the resulting seven benchmark datasets are shown in Table 1.

4.2 BENCHMARK METHODS

Network architectures. We employ Geometric Graph Neural Networks (GNNs) (Han et al., 2024), which are designed to process data with geometric structures and have been widely used

Table 2: Test MAE(↓) on the benchmark dataset where BalancedMSE is abbreviated to BMSE. Bold is for the best and italics is for the second best in each column for both models. We report the standard deviation among 3 runs, consistent across all subsequent tables.

Model	Algo	Formation Energy	Shear Modulus		Refractive Index		Phonons Mode Peak		Avg Rank
		bottom	bottom	top	bottom	top	bottom	top	
PaiNN	ERM	0.424(0.001)	0.613(0.089)	0.363(0.000)	0.275(0.007)	0.781(0.017)	0.820(0.005)	0.975(0.022)	6.4
	LDS	0.372(0.018)	0.524(0.001)	0.335(0.004)	0.264(0.004)	0.781(0.011)	0.844(0.029)	1.04(0.091)	4.9
	Ranksim	0.421(0.002)	0.540(0.001)	*0.246(0.030)*	0.267(0.004)	0.775(0.002)	*0.732(0.106)*	1.00(0.071)	4.4
	BMSE	*0.360(0.050)*	**0.462(0.041)**	**0.214(0.038)**	0.269(0.059)	*0.671(0.010)*	0.758(0.011)	1.02(0.018)	*3*
	ConR	0.432(0.056)	0.535(0.004)	0.329(0.002)	0.303(0.129)	0.807(0.051)	0.884(0.17)	0.974(0.073)	6.3
	C-Mixup	0.391(0.002)	0.539(0.001)	0.353(0.001)	0.258(0.002)	0.791(0.006)	0.848(0.010)	*0.966(0.013)*	5.1
	FOMA	0.419(0.005)	0.502(0.005)	0.351(0.043)	*0.239(0.046)*	0.746(0.020)	0.776(0.006)	1.09(0.109)	4.4
	MEX	**0.309(0.018)**	*0.481(0.014)*	0.298(0.008)	**0.177(0.019)**	**0.586(0.012)**	**0.567(0.008)**	**0.926(0.008)**	**1.4**
EquiformerV2	ERM	0.367(0.003)	0.512(0.001)	0.306(0.001)	0.218(0.001)	0.639(0.002)	0.730(0.006)	0.923(0.010)	5.6
	LDS	*0.278(0.008)*	0.4944(0.004)	0.295(0.005)	0.195(0.009)	0.643(0.002)	0.749(0.001)	0.905(0.012)	3.9
	Ranksim	0.366(0.004)	0.484(0.044)	0.306(0.004)	0.219(0.002)	0.647(0.008)	0.730(0.012)	0.916(0.003)	5.4
	BMSE	0.398(0.136)	*0.388(0.028)*	**0.167(0.020)**	*0.184(0.006)*	*0.599(0.013)*	*0.568(0.039)*	1.02(0.022)	*3.4*
	ConR	0.351(0.006)	0.509(0.004)	0.330(0.005)	0.224(0.004)	0.622(0.002)	0.765(0.003)	*0.897(0.009)*	5.6
	C-Mixup	0.316(0.009)	0.509(0.001)	0.319(0.003)	0.205(0.003)	0.628(0.008)	0.752(0.002)	0.915(0.005)	5.1
	FOMA	0.314(0.004)	0.512(0.004)	0.311(0.009)	0.196(0.004)	0.627(0.002)	0.768(0.020)	1.068(0.222)	5.9
	MEX	**0.172(0.008)**	**0.376(0.010)**	*0.245(0.020)*	**0.141(0.004)**	**0.501(0.018)**	**0.495(0.007)**	**0.789(0.011)**	**1.1**

Table 3: Test GM(↓) on the benchmark dataset where BalancedMSE is abbreviated to BMSE.

Model	Algo	Formation Energy	Shear Modulus		Refractive Index		Phonons Mode Peak		Avg Rank
		bottom	bottom	top	bottom	top	bottom	top	
PaiNN	ERM	0.388(0.001)	0.571(0.094)	0.340(0.001)	0.228(0.008)	0.709(0.020)	0.750(0.006)	0.849(0.020)	6.7
	LDS	0.337(0.019)	0.479(0.001)	0.310(0.003)	*0.178(0.003)*	0.668(0.008)	0.770(0.026)	0.910(0.098)	4.6
	Ranksim	0.385(0.002)	0.495(0.001)	*0.214(0.030)*	0.223(0.008)	0.659(0.0001)	0.646(0.123)	0.879(0.071)	4.9
	BMSE	*0.247(0.041)*	**0.367(0.041)**	**0.142(0.036)**	0.205(0.074)	*0.501(0.010)*	*0.581(0.018)*	*0.800(0.021)*	*2*
	ConR	0.385(0.076)	0.488(0.005)	0.306(0.002)	0.275(0.144)	0.737(0.061)	0.817(0.182)	0.845(0.082)	6.1
	C-Mixup	0.354(0.003)	0.493(0.001)	0.330(0.002)	0.213(0.002)	0.689(0.200)	0.781(0.012)	0.852(0.014)	5.6
	FOMA	0.383(0.005)	0.454(0.006)	0.331(0.045)	0.203(0.052)	0.634(0.019)	0.701(0.008)	0.979(0.120)	4.7
	MEX	**0.246(0.019)**	*0.432(0.016)*	0.272(0.009)	**0.126(0.024)**	**0.495(0.013)**	**0.423(0.035)**	**0.756(0.031)**	**1.4**
EquiformerV2	ERM	0.330(0.003)	0.466(0.001)	0.288(0.001)	0.172(0.001)	0.550(0.003)	0.667(0.008)	0.829(0.007)	5.9
	LDS	*0.236(0.010)*	0.446(0.004)	0.275(0.005)	0.136(0.0111)	0.555(0.003)	0.686(0.0011)	0.806(0.0087)	3.9
	Ranksim	0.329(0.004)	0.436(0.049)	0.288(0.004)	0.172(0.002)	0.561(0.010)	0.669(0.014)	0.825(0.006)	5.7
	BMSE	0.301(0.134)	**0.298(0.032)**	**0.110(0.019)**	*0.106(0.001)*	*0.456(0.015)*	*0.389(0.026)*	0.822(0.019)	*2.6*
	ConR	0.318(0.005)	0.465(0.004)	0.310(0.004)	0.180(0.005)	0.527(0.001)	0.704(0.003)	*0.800(0.010)*	5.7
	C-Mixup	0.279(0.009)	0.463(0.001)	0.302(0.003)	0.161(0.003)	0.537(0.008)	0.691(0.002)	0.820(0.005)	5
	FOMA	0.278(0.005)	0.467(0.004)	0.293(0.009)	0.141(0.006)	0.538(0.002)	0.709(0.021)	0.993(0.245)	6
	MEX	**0.113(0.006)**	*0.300(0.014)*	*0.208(0.025)*	**0.069(0.007)**	**0.364(0.030)**	**0.369(0.008)**	**0.631(0.014)**	**1.3**

in material property prediction. We selected two representative equivariant Geometric GNNs: PaiNN (Schütt et al., 2021) and EquiformerV2 (Liao et al., 2024) from `fairchem`[1] as the backbone for all benchmark methods.

Algorithms. Given the limited number of proposals for extrapolation in the literature, we explore two categories of extrapolative regression methods. The first category is DIR methods. The second is the regression data augmentation (DA). To provide a comprehensive evaluation, we assess the performance of several representative methods from each category. Specifically, we choose LDS (Yang et al., 2021), Ranksim (Gong et al., 2022), BalancedMSE (Ren et al., 2022), and Conr (Keramati et al., 2024) for DIR methods; C-Mixup (Yao et al., 2022) and FOMA (Kaufman & Azencot, 2024) for regression DA. All these methods are benchmarked against the empirical risk minimization (ERM) baseline to evaluate their performance.

Implementation details. MEX is a general training framework agnostic to the material encoder. For the label encoder of MEX, we employ a linear layer attached by an activation function. The score module is a 4-layer Multi-layer Perceptron (MLP) that projects the concatenated sample and label representation to a score scalar. Besides, we empirically investigate various implementations of and compare their performance in Section 4.5.

[1] `https://github.com/FAIR-Chem/fairchem?tab=readme-ov-file`

In the training phase, 500 noisy labels are sampled for each example. We simply follow Gustafsson et al. (2020) to set $K = 3$ and $\sigma_1 = 0.075, \sigma_2 = 0.15, \sigma_3 = 0.3$ for the noisy distribution. During inference, the candidate label size is established at $C = 1500$, which is initially sampled uniformly from $[\lfloor l \rfloor, \lceil u \rceil]$, where l and u are the lower bound and upper bound of the entire dataset label range. Note that this interval can be freely adjusted based on prior knowledge of material properties. The candidate labels are updated for 10 iterations before we make the final prediction.

For all experiments, models were trained for a maximum of 200 epochs, with early stopping applied if the validation mean absolute error (MAE) did not improve for 30 consecutive epochs. We employed the AdamW (Loshchilov & Hutter, 2019) optimizer in conjunction with a `ReduceLROnPlateau` learning rate schedule, which reduced the learning rate by a factor of 0.8 after 5 epochs without improvement. Hyper-parameter selection was performed based on validation MAE via grid search, with the trade-off parameter λ of MEX selected from $\{0.25, 0.5, 0.75, 1\}$, batch sizes from $\{32, 64, 128\}$, learning rates from $\{0.00005, 0.0001, 0.001\}$, and weight decay from $\{0, 0.001\}$. All methods were evaluated under three random seeds, and the average and standard deviation of MAE, error Geometric Mean (GM) (Yang et al., 2021), and Spearman correlation coefficient across all datasets were reported.

4.3 Main Results

We report the performance for all methods in Table 2 and Table 3.

MEX achieves superior extrapolation performance. As shown in Table 2 and Table 3, MEX attains the best average rank across all models and both metrics, with the lowest MAE on 5 out of 7 datasets for PaiNN and 6 out of 7 for EquiformerV2. Under GM, MEX demonstrates the highest performance on 4 datasets for PaiNN and 5 for EquiformerV2. On other datasets, such as Shear Modulus, MEX performs competitively with the best-performing BalancedMSE method.

DIR methods are strong baselines for extrapolation. We observe that all DIR methods rank better than ERM on average for both models. For each dataset, at least one DIR method outperforms ERM, demonstrating their effectiveness for extrapolation. Notably, among the DIR methods, BalancedMSE consistently achieves the highest rank. However, no single DIR method outperforms ERM across all datasets, highlighting the need for methods specifically designed for extrapolation in MPR. Nevertheless, we recommend that future evaluations consistently include DIR methods as baselines due to their overall robustness.

Regression DA helps extrapolation, but depends on models. In Table 2, C-Mixup and FOMA consistently outperform ERM for PaiNN, with average ranks of 5.1 and 4.4, respectively, compared to 6.4 for ERM. However, their advantage diminishes when applied to EquiformerV2, where FOMA performs worse than ERM (rank 5.9 vs. 5.6). Although C-Mixup demonstrates better overall performance, the improvements on certain datasets, such as Shear Modulus (bottom), are marginal. A similar trend is observed under GM metrics (Table 3). This variability may arise from our application of augmentation in the feature space. Since different models produce latent representations of varying quality, the effectiveness of data augmentation methods fluctuates accordingly. This underscores the importance of developing robust material representation models, which are crucial for the success of feature-based data augmentation techniques. Additionally, it is interesting to design material-specific augmentation methods beyond those designed solely for continuous input data.

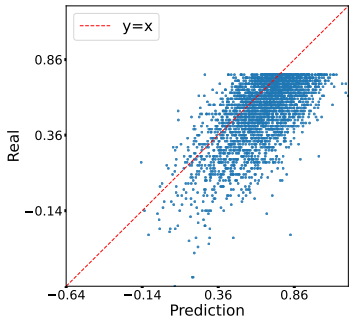

Figure 4: Prediction result of MEX on the test set of Formation Energy (bottom).

Extrapolation remains a challenging problem. The MAEs on our extrapolation benchmark are significantly larger than those obtained under random splits (Dunn et al., 2020). For instance, the early CGCNN (Xie & Grossman, 2018) achieves an MAE of 0.0452 (as reported by Dunn et al. (2020)) on the Formation Energy dataset under random split, which is considerably smaller than the smallest MAE (0.172, detailed results in Figure 4) under our extrapolative split configuration.

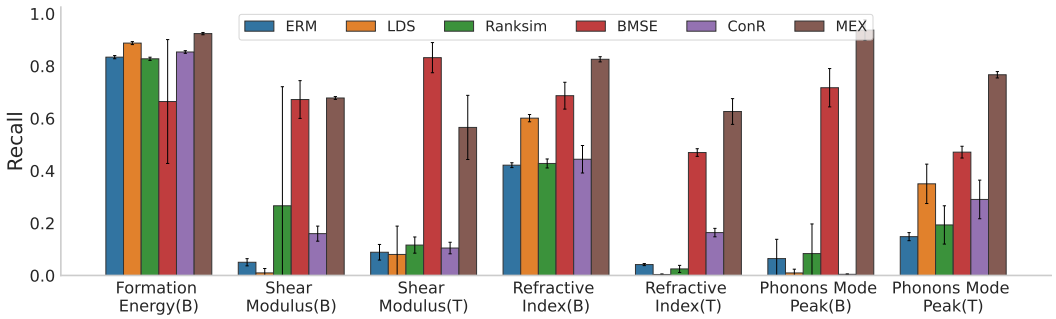

Figure 5: Recall rate of MEX and five DIR methods in detecting extrapolative samples.

To take a closer look at the prediction performance, we also calculate the Spearman correlation between the predictions and the target. We find that all methods exhibit weak (0-0.4) or even negative correlations with the targets across most datasets (quantization results are listed in Appendix Table 6). However, for the Formation Energy dataset, most methods achieve stronger correlations, which we hypothesize is due to the availability of sufficient data and the relative simplicity of the material structure in this task. In conclusion, accurate prediction for extrapolative samples remains extremely challenging for current methods.

4.4 Potential impact on cutting-edge material discovery

As discussed in Section 4.3, extrapolation presents a significant challenge for methods in the literature, and our approach is no exception. Given the inherent limitations of neural networks in extrapolating (Xu et al., 2021), one may wonder: *To what extent can current deep learning methods assist in the discovery of cutting-edge materials?*

In addition to accurately predicting the property values of extrapolative samples, we contend that the ability to **detect** materials with potentially groundbreaking properties is also crucial. Once identified, these candidates can be further refined using first-principles methods, such as Density Functional Theory (DFT), to compute more precise properties. Consequently, models' detection capabilities could become vital tools in advancing material discovery.

To assess the effectiveness of different methods in detecting materials within extrapolation regions, we present their recall rates in Figure 5. Specifically, for samples from the validation and test sets in our benchmark, a sample is considered detected if its predicted value falls within the extrapolation interval, and the recall rate is calculated as the proportion of such samples correctly identified. As shown, MEX outperforms previous methods in 6 out of 7 detection tasks. Notably, it achieves a recall rate of over 80% on three datasets and exceeds 60% on six datasets. This substantial performance advantage demonstrates the robustness of MEX and highlights its potential to identify cutting-edge materials that might otherwise be overlooked.

4.5 Discussion

Score module analysis. The score module is a critical component in learning fine-grained relationships between sample and label. Here, we investigate the effects of various design choices. The first, referred to as MEX (mlp+cos), employs two independent 2-layer MLPs to project the sample and label representations into a new space, after which the cosine similarity between the two projections is computed. The second approach, MEX (cos), directly computes the cosine similarity between the original sample and label representations. As illustrated in Table 4, MEX and MEX (mlp+cos) exhibit comparable performance, while MEX (cos) demonstrates inferior performance relative to the other designs. This observation aligns with findings in SimCLR (Chen et al., 2020), which indicate that incorporating a learnable nonlinear transformation on the representations before applying the contrastive loss, rather than directly optimizing the representations, significantly enhances the quality of the learned features.

Table 4: Test MAE and GM of EquiformerV2 on Formation Energy, Refeactive Index(bottom& top) datasets. MEX (cos) and MEX (mlp+cos) denote different designs of the score module in our framework.

Metrics	MAE(↓)			GM(↓)		
Dataset	Formation Energy	Refractive Index		Formation Energy	Refractive Index	
	bottom	bottom	top	bottom	bottom	top
MEX (cos)	0.382(0.004)	0.231(0.003)	0.625(0.007)	0.346(0.004)	0.184(0.004)	0.533(0.005)
MEX (mlp+cos)	**0.169(0.014)**	0.170(0.003)	0.518(0.009)	**0.112(0.011)**	0.100(0.005)	0.373(0.013)
MEX	0.172(0.008)	**0.141(0.004)**	**0.501(0.018)**	0.113(0.006)	**0.069(0.007)**	**0.364(0.030)**

Trade-off parameter analysis. We examine the selection of the trade-off parameter λ by assessing model performance across various values of λ. Figure 6 illustrates the performance of MEX alongside prior top-performing methods on three benchmark datasets. As λ changes, MEX consistently surpasses previous approaches across both models, thereby confirming its robustness to diverse hyperparameter configurations and backbone architecture choices.

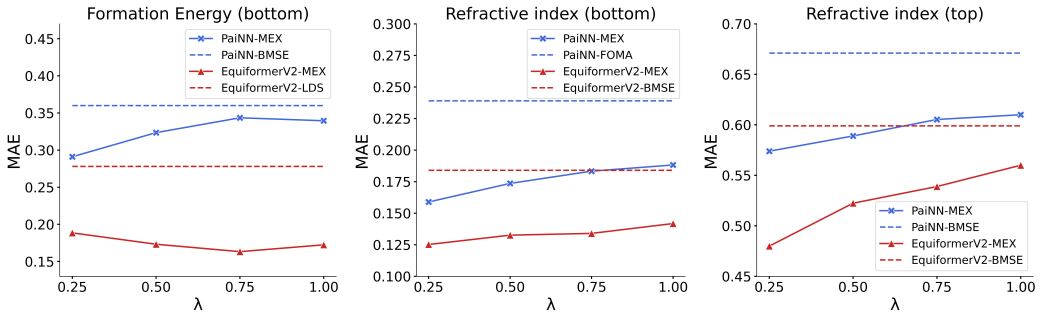

Figure 6: Ablation study on the trading-off parameter λ.

Running time analysis. Our method requires an iterative refinement of candidate labels before making the final prediction for each testing sample, which inherently results in a longer processing time compared to traditional regression methods. Specifically, this involves encoding 1,500 labels and computing their matching value over 10 iterations during our experiment. Despite this complexity, our experimental results indicate that the average computation time for MEX per test sample is about 0.006s on the NVIDIA 3090, which is comparable to baseline methods (around 0.002s). Thus, the computational overhead associated with our approach remains acceptable.

5 CONCLUSION

In this work, we shed light on the challenging task of extrapolation in material property regression (MPR), which aims to generalize to materials with unseen property values. We introduce a new benchmark consisting of seven MPR tasks and provide a comprehensive evaluation of existing methods' extrapolation capabilities. To address the task, we propose a simple yet effective framework that captures the sample-label matching relationship in the latent space. Extensive experiments demonstrate the superior performance of our approach and highlight its potential application in the discovery of cutting-edge materials.

REFERENCES

Paula Branco, Luís Torgo, and Rita P. Ribeiro. SMOGN: a pre-processing approach for imbalanced regression. In *First International Workshop on Learning with Imbalanced Domains: Theory and Applications, LIDTA@PKDD/ECML 2017, 22 September 2017, Skopje, Macedonia*, volume 74 of *Proceedings of Machine Learning Research*, pp. 36–50. PMLR, 2017. URL `http://proceedings.mlr.press/v74/branco17a.html`.

Ivano E Castelli, David D Landis, Kristian S Thygesen, Søren Dahl, Ib Chorkendorff, Thomas F Jaramillo, and Karsten W Jacobsen. New cubic perovskites for one-and two-photon water splitting using the computational materials repository. *Energy & Environmental Science*, 5(10):9034–9043, 2012a.

Ivano E Castelli, Thomas Olsen, Soumendu Datta, David D Landis, Søren Dahl, Kristian S Thygesen, and Karsten W Jacobsen. Computational screening of perovskite metal oxides for optimal solar light capture. *Energy & Environmental Science*, 5(2):5814–5819, 2012b.

Rees Chang, Yu-Xiong Wang, and Elif Ertekin. Towards overcoming data scarcity in materials science: unifying models and datasets with a mixture of experts framework. *npj Computational Materials*, 8(1):242, 2022.

Ting Chen, Simon Kornblith, Mohammad Norouzi, and Geoffrey E. Hinton. A simple framework for contrastive learning of visual representations. In *Proceedings of the 37th International Conference on Machine Learning, ICML 2020, 13-18 July 2020, Virtual Event*, volume 119 of *Proceedings of Machine Learning Research*, pp. 1597–1607. PMLR, 2020. URL http://proceedings.mlr.press/v119/chen20j.html.

Kamal Choudhary, Daniel Wines, Kangming Li, Kevin F Garrity, Vishu Gupta, Aldo H Romero, Jaron T Krogel, Kayahan Saritas, Addis Fuhr, Panchapakesan Ganesh, et al. Jarvis-leaderboard: a large scale benchmark of materials design methods. *npj Computational Materials*, 10(1):93, 2024.

Alexander Dunn, Qi Wang, Alex Ganose, Daniel Dopp, and Anubhav Jain. Benchmarking materials property prediction methods: the matbench test set and automatminer reference algorithm. *npj Computational Materials*, 6(1):138, 2020.

Johannes Gasteiger, Florian Becker, and Stephan Günnemann. Gemnet: Universal directional graph neural networks for molecules. In Marc'Aurelio Ranzato, Alina Beygelzimer, Yann N. Dauphin, Percy Liang, and Jennifer Wortman Vaughan (eds.), *Advances in Neural Information Processing Systems 34: Annual Conference on Neural Information Processing Systems 2021, NeurIPS 2021, December 6-14, 2021, virtual*, pp. 6790–6802, 2021. URL https://proceedings.neurips.cc/paper/2021/hash/35cf8659cfcb13224cbd47863a34fc58-Abstract.html.

Yu Gong, Greg Mori, and Frederick Tung. Ranksim: Ranking similarity regularization for deep imbalanced regression. In Kamalika Chaudhuri, Stefanie Jegelka, Le Song, Csaba Szepesvári, Gang Niu, and Sivan Sabato (eds.), *International Conference on Machine Learning, ICML 2022, 17-23 July 2022, Baltimore, Maryland, USA*, volume 162 of *Proceedings of Machine Learning Research*, pp. 7634–7649. PMLR, 2022. URL https://proceedings.mlr.press/v162/gong22a.html.

Fredrik Gustafsson, Martin Danelljan, Radu Timofte, and Thomas B. Schön. How to train your energy-based model for regression. In *31st British Machine Vision Conference 2020, BMVC 2020, Virtual Event, UK, September 7-10, 2020*. BMVA Press, 2020. URL https://www.bmvc2020-conference.com/assets/papers/0154.pdf.

Michael Gutmann and Aapo Hyvärinen. Noise-contrastive estimation: A new estimation principle for unnormalized statistical models. In Yee Whye Teh and D. Mike Titterington (eds.), *Proceedings of the Thirteenth International Conference on Artificial Intelligence and Statistics, AISTATS 2010, Chia Laguna Resort, Sardinia, Italy, May 13-15, 2010*, volume 9 of *JMLR Proceedings*, pp. 297–304. JMLR.org, 2010. URL http://proceedings.mlr.press/v9/gutmann10a.html.

Jiaqi Han, Jiacheng Cen, Liming Wu, Zongzhao Li, Xiangzhe Kong, Rui Jiao, Ziyang Yu, Tingyang Xu, Fandi Wu, Zihe Wang, Hongteng Xu, Zhewei Wei, Yang Liu, Yu Rong, and Wenbing Huang. A survey of geometric graph neural networks: Data structures, models and applications. *CoRR*, abs/2403.00485, 2024. doi: 10.48550/ARXIV.2403.00485. URL https://doi.org/10.48550/arXiv.2403.00485.

Tito Homem-de Mello and Güzin Bayraksan. Monte carlo sampling-based methods for stochastic optimization. *Surveys in Operations Research and Management Science*, 19(1):56–85, 2014.

A Jain, SP Ong, G Hautier, W Chen, WD Richards, S Dacek, S Cholia, D Gunter, D Skinner, G Ceder, et al. The materials project: a materials genome approach to accelerating materials innovation. apl mater 1: 011002, 2013.

Ilya Kaufman and Omri Azencot. First-order manifold data augmentation for regression learning. In *Forty-first International Conference on Machine Learning, ICML 2024, Vienna, Austria, July 21-27, 2024*. OpenReview.net, 2024. URL https://openreview.net/forum?id=geajNKab7g.

Mahsa Keramati, Lili Meng, and R. David Evans. Conr: Contrastive regularizer for deep imbalanced regression. In *The Twelfth International Conference on Learning Representations, ICLR 2024, Vienna, Austria, May 7-11, 2024*. OpenReview.net, 2024. URL https://openreview.net/forum?id=RIuevDSK5V.

Hyung Jong Kim and Takuma Yasuda. Narrowband emissive thermally activated delayed fluorescence materials. *Advanced Optical Materials*, 10(22):2201714, 2022.

Johannes Klicpera, Janek Groß, and Stephan Günnemann. Directional message passing for molecular graphs. In *8th International Conference on Learning Representations, ICLR 2020, Addis Ababa, Ethiopia, April 26-30, 2020*. OpenReview.net, 2020. URL https://openreview.net/forum?id=B1eWbxStPH.

Yi-Lun Liao, Brandon M. Wood, Abhishek Das, and Tess E. Smidt. Equiformerv2: Improved equivariant transformer for scaling to higher-degree representations. In *The Twelfth International Conference on Learning Representations, ICLR 2024, Vienna, Austria, May 7-11, 2024*. OpenReview.net, 2024. URL https://openreview.net/forum?id=mCOBKZmrzD.

Ilya Loshchilov and Frank Hutter. Decoupled weight decay regularization. In *7th International Conference on Learning Representations, ICLR 2019, New Orleans, LA, USA, May 6-9, 2019*. OpenReview.net, 2019. URL https://openreview.net/forum?id=Bkg6RiCqY7.

Saro Passaro and C. Lawrence Zitnick. Reducing SO(3) convolutions to SO(2) for efficient equivariant gnns. In Andreas Krause, Emma Brunskill, Kyunghyun Cho, Barbara Engelhardt, Sivan Sabato, and Jonathan Scarlett (eds.), *International Conference on Machine Learning, ICML 2023, 23-29 July 2023, Honolulu, Hawaii, USA*, volume 202 of *Proceedings of Machine Learning Research*, pp. 27420–27438. PMLR, 2023. URL https://proceedings.mlr.press/v202/passaro23a.html.

Ioannis Petousis, David Mrdjenovich, Eric Ballouz, Miao Liu, Donald Winston, Wei Chen, Tanja Graf, Thomas D Schladt, Kristin A Persson, and Fritz B Prinz. High-throughput screening of inorganic compounds for the discovery of novel dielectric and optical materials. *Scientific data*, 4(1):1–12, 2017.

Guido Petretto, Shyam Dwaraknath, Henrique PC Miranda, Donald Winston, Matteo Giantomassi, Michiel J Van Setten, Xavier Gonze, Kristin A Persson, Geoffroy Hautier, and Gian-Marco Rignanese. High-throughput density-functional perturbation theory phonons for inorganic materials. *Scientific data*, 5(1):1–12, 2018.

Jiawei Ren, Mingyuan Zhang, Cunjun Yu, and Ziwei Liu. Balanced MSE for imbalanced visual regression. In *IEEE/CVF Conference on Computer Vision and Pattern Recognition, CVPR 2022, New Orleans, LA, USA, June 18-24, 2022*, pp. 7916–7925. IEEE, 2022. doi: 10.1109/CVPR52688.2022.00777. URL https://doi.org/10.1109/CVPR52688.2022.00777.

Kristof Schütt, Oliver T. Unke, and Michael Gastegger. Equivariant message passing for the prediction of tensorial properties and molecular spectra. In Marina Meila and Tong Zhang (eds.), *Proceedings of the 38th International Conference on Machine Learning, ICML 2021, 18-24 July 2021, Virtual Event*, volume 139 of *Proceedings of Machine Learning Research*, pp. 9377–9388. PMLR, 2021. URL http://proceedings.mlr.press/v139/schutt21a.html.

Kristof T Schütt, Huziel E Sauceda, P-J Kindermans, Alexandre Tkatchenko, and K-R Müller. Schnet–a deep learning architecture for molecules and materials. *The Journal of Chemical Physics*, 148(24), 2018.

Nima Shoghi, Adeesh Kolluru, John R. Kitchin, Zachary W. Ulissi, C. Lawrence Zitnick, and Brandon M. Wood. From molecules to materials: Pre-training large generalizable models for atomic property prediction. In *The Twelfth International Conference on Learning Representations, ICLR 2024, Vienna, Austria, May 7-11, 2024*. OpenReview.net, 2024. URL https://openreview.net/forum?id=PfPnugdxup.

Zixing Song, Ziqiao Meng, and Irwin King. A diffusion-based pre-training framework for crystal property prediction. In Michael J. Wooldridge, Jennifer G. Dy, and Sriraam Natarajan (eds.), *Thirty-Eighth AAAI Conference on Artificial Intelligence, AAAI 2024, Thirty-Sixth Conference on Innovative Applications of Artificial Intelligence, IAAI 2024, Fourteenth Symposium on Educational Advances in Artificial Intelligence, EAAI 2014, February 20-27, 2024, Vancouver, Canada*, pp. 8993–9001. AAAI Press, 2024. doi: 10.1609/AAAI.V38I8.28748. URL https://doi.org/10.1609/aaai.v38i8.28748.

Michael Steininger, Konstantin Kobs, Padraig Davidson, Anna Krause, and Andreas Hotho. Density-based weighting for imbalanced regression. *Mach. Learn.*, 110(8):2187–2211, 2021. doi: 10.1007/S10994-021-06023-5. URL https://doi.org/10.1007/s10994-021-06023-5.

Luís Torgo, Rita P. Ribeiro, Bernhard Pfahringer, and Paula Branco. SMOTE for regression. In Luís Correia, Luís Paulo Reis, and José Cascalho (eds.), *Progress in Artificial Intelligence - 16th Portuguese Conference on Artificial Intelligence, EPIA 2013, Angra do Heroísmo, Azores, Portugal, September 9-12, 2013. Proceedings*, volume 8154 of *Lecture Notes in Computer Science*, pp. 378–389. Springer, 2013. doi: 10.1007/978-3-642-40669-0_33. URL https://doi.org/10.1007/978-3-642-40669-0_33.

Ziyan Wang and Hao Wang. Variational imbalanced regression: Fair uncertainty quantification via probabilistic smoothing. In Alice Oh, Tristan Naumann, Amir Globerson, Kate Saenko, Moritz Hardt, and Sergey Levine (eds.), *Advances in Neural Information Processing Systems 36: Annual Conference on Neural Information Processing Systems 2023, NeurIPS 2023, New Orleans, LA, USA, December 10 - 16, 2023*, 2023. URL http://papers.nips.cc/paper_files/paper/2023/hash/612a56f193d031687683445cd0001083-Abstract-Conference.html.

Logan Ward, Alexander Dunn, Alireza Faghaninia, Nils ER Zimmermann, Saurabh Bajaj, Qi Wang, Joseph Montoya, Jiming Chen, Kyle Bystrom, Maxwell Dylla, et al. Matminer: An open source toolkit for materials data mining. *Computational Materials Science*, 152:60–69, 2018.

Tian Xie and Jeffrey C Grossman. Crystal graph convolutional neural networks for an accurate and interpretable prediction of material properties. *Physical review letters*, 120(14):145301, 2018.

Keyulu Xu, Mozhi Zhang, Jingling Li, Simon Shaolei Du, Ken-ichi Kawarabayashi, and Stefanie Jegelka. How neural networks extrapolate: From feedforward to graph neural networks. In *9th International Conference on Learning Representations, ICLR 2021, Virtual Event, Austria, May 3-7, 2021*. OpenReview.net, 2021. URL https://openreview.net/forum?id=UH-cmocLJC.

Yincai Xu, Zong Cheng, Zhiqiang Li, Baoyan Liang, Jiaxuan Wang, Jinbei Wei, Zuolun Zhang, and Yue Wang. Molecular-structure and device-configuration optimizations toward highly efficient green electroluminescence with narrowband emission and high color purity. *Advanced Optical Materials*, 8(9):1902142, 2020.

Keqiang Yan, Yi Liu, Yuchao Lin, and Shuiwang Ji. Periodic graph transformers for crystal material property prediction. In Sanmi Koyejo, S. Mohamed, A. Agarwal, Danielle Belgrave, K. Cho, and A. Oh (eds.), *Advances in Neural Information Processing Systems 35: Annual Conference on Neural Information Processing Systems 2022, NeurIPS 2022, New Orleans, LA, USA, November 28 - December 9, 2022*, 2022. URL http://papers.nips.cc/paper_files/paper/2022/hash/6145c70a4a4bf353a31ac5496a72a72d-Abstract-Conference.html.

Yuzhe Yang, Kaiwen Zha, Ying-Cong Chen, Hao Wang, and Dina Katabi. Delving into deep imbalanced regression. In Marina Meila and Tong Zhang (eds.), *Proceedings of the 38th International Conference on Machine Learning, ICML 2021, 18-24 July 2021, Virtual Event*, volume 139 of *Proceedings of Machine Learning Research*, pp. 11842–11851. PMLR, 2021. URL http://proceedings.mlr.press/v139/yang21m.html.

Huaxiu Yao, Yiping Wang, Linjun Zhang, James Y. Zou, and Chelsea Finn. C-mixup: Improving generalization in regression. In Sanmi Koyejo, S. Mohamed, A. Agarwal, Danielle Belgrave, K. Cho, and A. Oh (eds.), *Advances in Neural Information Processing Systems 35: Annual Conference on Neural Information Processing Systems 2022, NeurIPS 2022, New Orleans, LA, USA, November 28 - December 9, 2022*, 2022. URL http://papers.nips.cc/paper_files/paper/2022/hash/1626be0ab7f3d7b3c639fbfd5951bc40-Abstract-Conference.html.

Duo Zhang, Xinzijian Liu, Xiangyu Zhang, Chengqian Zhang, Chun Cai, Hangrui Bi, Yiming Du, Xuejian Qin, Jiameng Huang, Bowen Li, et al. Dpa-2: Towards a universal large atomic model for molecular and material simulation. *arXiv preprint arXiv:2312.15492*, 2023.

Shihao Zhang, Kenji Kawaguchi, and Angela Yao. Deep regression representation learning with topology. In *Forty-first International Conference on Machine Learning, ICML 2024, Vienna, Austria, July 21-27, 2024*. OpenReview.net, 2024. URL https://openreview.net/forum?id=HbdeEGVfEN.

A Appendix

A.1 Dataset characteristics

Table 5: Dataset characteristics, including total atom types, atom numbers (mean and std.), and lattice constants (mean and std.). The symbols $\boldsymbol{a}$, $\boldsymbol{b}$, and $\boldsymbol{c}$ denote the unit cell vectors. The notation $\|\cdot\|$ denotes the length of a vector and $\angle(\cdot,\cdot)$ denotes the angle between two vectors.

Property	Atom Types	Atom Num.	$\|\boldsymbol{a}\|$	$\|\boldsymbol{b}\|$	$\|\boldsymbol{c}\|$	$\angle(\boldsymbol{b},\boldsymbol{c})$	$\angle(\boldsymbol{a},\boldsymbol{c})$	$\angle(\boldsymbol{a},\boldsymbol{b})$
Formation Energy	56	5 (0)	4.14 (0.31)	4.14 (0.31)	4.14 (0.31)	90.0 (0)	90.0 (0)	90.0 (0)
Shear Modulus	84	8.63 (8.66)	4.96 (1.5)	5.33 (1.67)	6.41 (2.98)	83.29 (20.3)	82.86 (19.78)	85.35 (23.49)
Refractive Index	80	16.9 (14.67)	5.98 (1.94)	6.6 (2.31)	7.98 (3.61)	86.32 (19.39)	87.07 (19.12)	89.55 (22.47)
Phonons Mode Peak	64	7.53 (3.74)	5.32 (1.42)	5.66 (1.57)	6.72 (2.09)	83.55 (23.85)	82.95 (23.4)	84.1 (25.15)

A.2 Inference algorithm

Algorithm 1: Inference by Monte Carlo Sampling-Based Stochastic Optimization

Input: x: Input sample, $\mathcal{M}$: Matching function, C: Number of candidate labels, T: Iterations, l: Lower bound of label range, u: Upper bound of label range, β: noise shrink factor
Output: $y^\star$: Optimal label
$ns \leftarrow$ initial noise scale;
$\{y_i \sim \mathcal{U}(l,u)\}_{i=1}^{C} \leftarrow$ initial labels;
`// uniform sample from` $[l,u]$
for $t \leftarrow 1$ **to** T **do**
  $\{p_i\}_{i=1}^{C} \leftarrow \text{Softmax}(\{\mathcal{M}(x,y_i)\}_{i=1}^{C})$
  $\{y_i\}_{i=1}^{C} \leftarrow \text{sample}(\{y_i\}_{i=1}^{C}, \{p_i\}_{i=1}^{C})$;
  `// Sampling based on probability with replacement`
  for $i \leftarrow 1$ **to** C **do**
    $\epsilon_i \sim \mathcal{N}(0,1)$;
    $y_i \leftarrow y_i + \epsilon_i * ns$;
    $y_i \leftarrow \text{clip}(y_i, l, u)$;
    `// clip` y_i `to` $[l,u]$
  end
  $ns \leftarrow \beta * ns$;
  `// shrink noise scale`
end
$y^\star \leftarrow \text{argmax}_{y \in \{y_i\}_{i=1}^{C}} \mathcal{M}(x,y)$;
return $y^\star$;

A.3 Additional Results

A.3.1 Spearman coefficient for all methods

Table 6: Test Spearman correlation efficient on the benchmark dataset where BalancedMSE is abbreviated to BMSE.

Model	Algo	Formation Energy	Shear Modulus		Refractive Index		Phonons Mode Peak	
		bottom	bottom	top	bottom	top	bottom	top
PaiNN	ERM	0.541(0.005)	0.059(0.148)	-0.128(0.047)	-0.116(0.039)	-0.208(0.065)	**-0.181(0.007)**	-0.421(0.004)
	LDS	**0.660(0.013)**	0.171(0.028)	-0.022(0.080)	-0.104(0.024)	-0.265(0.018)	-0.230(0.043)	-0.379(0.018)
	Ranksim	0.542(0.004)	0.170(0.017)	-0.018(0.023)	-0.070(0.0430)	-0.314(0.009)	-0.216(0.046)	-0.418(0.012)
	BMSE	0.351(0.044)	0.099(0.064)	-0.054(0.055)	-0.133(0.066)	-0.237(0.022)	-0.260(0.054)	**-0.302(0.017)**
	ConR	0.473(0.101)	0.131(0.019)	-0.032(0.033)	0.009(0.029)	-0.174(0.036)	-0.210(0.029)	-0.430(0.018)
	C-Mixup	0.567(0.005)	0.144(0.019)	-0.093(0.017)	-0.052(0.016)	-0.213(0.129)	**-0.181(0.010)**	-0.437(0.014)
	FOMA	0.534(0.013)	0.232(0.020)	-0.046(0.080)	**0.093(0.018)**	-0.325(0.005)	-0.205(0.044)	-0.384(0.042)
	MEX	0.489(0.051)	**0.319(0.015)**	**0.042(0.003)**	0.059(0.027)	**0.039(0.039)**	-0.201(0.038)	-0.335(0.018)
EquiformerV2	ERM	0.615(0.015)	0.336(0.042)	0.069(0.024)	0.194(0.015)	-0.120(0.016)	0.008(0.054)	-0.459(0.011)
	LDS	0.71(0.044)	0.155(0.033)	0.020(0.085)	**0.237(0.020)**	-0.031(0.013)	0.009(0.117)	-0.411(0.030)
	Ranksim	0.625(0.014)	0.332(0.009)	0.094(0.016)	0.195(0.021)	-0.060(0.004)	**0.061(0.071)**	-0.432(0.015)
	BMSE	0.273(0.043)	0.278(0.033)	0.074(0.020)	-0.016(0.004)	-0.126(0.0470)	-0.175(0.037)	-0.393(0.003)
	ConR	**0.724(0.012)**	0.357(0.023)	0.109(0.038)	-0.021(0.047)	-0.022(0.008)	-0.050(0.108)	-0.460(0.047)
	C-Mixup	0.682(0.019)	0.328(0.063)	0.117(0.055)	0.183(0.077)	-0.045(0.014)	0.005(0.003)	-0.479(0.008)
	FOMA	0.703(0.004)	0.317(0.032)	**0.131(0.060)**	0.211(0.028)	-0.012(0.003)	0.040(0.042)	**-0.360(0.184)**
	MEX	0.645(0.020)	**0.374(0.021)**	0.095(0.027)	0.080(0.027)	**0.088(0.006)**	-0.039(0.085)	-0.427(0.019)